Suppression of store-operated calcium entry causes dilated cardiomyopathy of the *Drosophila* heart

Courtney E. Petersen[1], Matthew J. Wolf[2], and Jeremy T. Smyth[3*]

[1]Graduate Program in Molecular and Cellular Biology and [3]Department of Anatomy, Physiology, and Genetics, Uniformed Services University of the Health Sciences, F. Edward Hébert School of Medicine, Bethesda, MD 20814

[2]Division of Cardiovascular Medicine, Department of Medicine, The University of Virginia School of Medicine, Charlottesville, VA 22908

[*]Corresponding Author:

Jeremy T. Smyth
Uniformed Services University of the Health Sciences
4301 Jones Bridge Rd
Bethesda, MD 20814
Tel: (301) 295-5879
Email: jeremy.smyth@usuhs.edu

ABSTRACT

Store-operated Ca^{2+} entry (SOCE) is an essential Ca^{2+} signaling and homeostatic mechanism present in nearly all animal cells. SOCE refers to Ca^{2+} influx into cells that is activated by depletion of endoplasmic or sarcoplasmic reticulum stores (ER/SR). In the SOCE pathway, Stim proteins function as Ca^{2+} sensors in the ER, and upon ER Ca^{2+} store depletion Stim rearranges to ER-plasma membrane junctional sites where it activates Orai Ca^{2+} influx channels. Multiple studies have implicated Stim and Orai mediated SOCE in heart pathophysiology. Importantly however, the specific functional roles of SOCE in cardiomyocytes have not been well elucidated. We have begun to address this in *Drosophila melanogaster*, a powerful model of cardiac development and physiology. We found that heart specific suppression of *Drosophila Stim* and *Orai* by RNAi using two independent *Gal4* drivers, *tinC-GAL4* and *4xhand-GAL4*, resulted in dilated cardiomyopathy, characterized by increased end diastolic and end systolic dimensions and decreased fractional shortening. Animals with heart specific *Stim* and *Orai* suppression also exhibited significant delays in development to pupal and adult stages, and adults died significantly earlier than controls, suggesting pathological effects of compromised cardiac output. Myofibers in *Stim* and *Orai* suppressed hearts were highly disorganized compared to controls in both larvae and adults, suggesting possible defects in heart development or upregulation of stress responses due to SOCE suppression. Collectively, our results demonstrate an essential role for SOCE in normal heart physiology, and establish *Drosophila* as an important model for future studies aimed at delineating functional SOCE roles in cardiomyocytes.

INTRODUCTION

Cardiac disease continues to be a leading cause of morbidity and mortality throughout the western world with current treatment options limited to palliative pharmacological or invasive therapy (McKenna et al., 2017). The discovery of curative treatments will rely on thorough understanding of the molecular mechanisms that govern onset and progression of cardiac pathophysiology. Significantly, irregularities in cardiomyocyte calcium (Ca^{2+}) homeostasis are a major contributing factor to cardiac disease pathogenesis and targeting Ca^{2+} signaling mechanisms may therefore be an important approach to novel therapeutic development (Abraham and Wolf, 2013; Kranias and Bers, 2007; Limas et al., 1987; MacLeod, 2016).

The role of Ca^{2+} in the process of excitation-contraction (E-C) coupling that drives cardiomyocyte contractility is well established. In E-C coupling, membrane depolarization opens L-type voltage gated Ca^{2+} channels and entering Ca^{2+} then activates ryanodine receptors (RyRs) in the sarcoplasmic reticulum (SR) membrane. Release of SR Ca^{2+} via RyRs results in a large cytoplasmic Ca^{2+} pulse that drives acto-myosin contractility (Bers, 2002). Importantly, Ca^{2+} homeostasis and functions in cardiomyocytes involve numerous other regulatory pathways in addition to E-C coupling. However, the functional roles of these Ca^{2+} regulatory pathways remain poorly understood. This includes the store operated Ca^{2+} entry (SOCE) pathway, which regulates the influx of Ca^{2+} into the cell upon depletion of internal sarco/endoplasmic reticulum (SR/ER) stores (Putney, 2011).

The main components of the SOCE pathway are Stim (stromal interacting molecule) and Orai. Stim is a single pass transmembrane protein that serves as a luminal ER/SR Ca^{2+} sensor, and Orai is a SOCE pore forming channel subunit on the plasma membrane. Pathway activation occurs upon depletion of ER/SR Ca^{2+} stores, resulting in the release of Ca^{2+} from the luminal N-terminus of Stim and subsequent Stim oligomerization. Oligomerized Stim then moves to ER-plasma membrane junctions where it interacts with and activates Orai to induce extracellular Ca^{2+} influx (Putney, 2018; Smyth et al., 2010). Ca^{2+} entering through the SOCE pathway can

then be pumped back into the ER/SR to replenish depleted stores. In addition to store refilling, SOCE Ca^{2+} can perform a multitude of other functions within the cell including regulation of gene expression, contractility, and maintenance of organelle function (Lacruz and Feske, 2015; Putney, 2018). In mammals, there are two Stim isoforms, Stim1 and Stim2, and three Orai isoforms (Orai1-3). Importantly, several studies have demonstrated an essential role for STIM1 and Orai1 mediated SOCE in the pathogenesis of pathological cardiac hypertrophy. For example, induction of cardiac hypertrophy by pressure overload results in upregulation of STIM1 and Orai1 expression in cardiomyocytes *in vivo*, and STIM1 and Orai1 suppression attenuates the hypertrophic response (Benard et al., 2016; Hulot et al., 2011; Luo et al., 2012; Parks et al., 2016). Similarly, suppression of STIM1 or Orai1 in rodent cardiomyocytes attenuates phenylephrine and endothelin-1 induced hypertrophy (Hulot et al., 2011; Luo et al., 2012; Voelkers et al., 2010). These results clearly demonstrate that SOCE signaling is required for pathological cardiac hypertrophy. However, whether SOCE is required in cardiomyocytes for normal cardiac physiology is far less clear. Cardiac restricted knockout of STIM1 in mouse resulted in marked left ventricular dilation in adults (Collins et al., 2014; Horton et al., 2014; Parks et al., 2016), concomitant with indications of ER stress and mitochondrial morphological changes. In addition, Orai1 suppression by antisense oligonucleotides in zebrafish resulted in sarcomeric abnormalities and reduced systolic function (Volkers et al., 2012). These results support the conclusion that SOCE is essential for normal cardiac physiology, but the specific cellular processes that are regulated by SOCE in cardiomyocytes are not known. The goal of our current study was to determine whether SOCE is required for heart function in *Drosophila melanogaster* and lay the groundwork for *in vivo* functional and genetic analyses of the mechanistic roles of SOCE in this powerful animal model.

Drosophila have emerged as an important tool in cardiac research due to their integration of well conserved developmental and physiological mechanisms with targeted genetic manipulation and *in vivo* analysis of heart function (Piazza and Wessells, 2011; Wolf et

al., 2006). The *Drosophila* heart, also referred to as the dorsal vessel, is a linear muscularized tube that runs along the dorsal midline of the animal and pumps hemolymph throughout the body in an open circulatory system (Rotstein and Paululat, 2016). Importantly, *Drosophila* express single isoforms of STIM and Orai, thus precluding issues of functional overlap seen with the multiple STIM and Orai isoforms in vertebrate models. Using this model, we demonstrate that animals with heart-specific suppression of the key SOCE pathway components, *Stim* and *Orai*, exhibit dilated cardiomyopathy characterized by enlarged end-diastolic and end-systolic dimensions and decreased fractional shortening. These animals also had a significant delay in development and ultimately died considerably earlier than controls, suggesting pathological impairment of cardiac function. Furthermore, *Stim* and *Orai* suppressed hearts exhibited highly disorganized or disrupted myofibrils, suggesting either defective heart development, tissue remodeling, or degeneration resulting from disrupted Ca^{2+} homeostasis. Collectively, these results, as well as results from other animal models, demonstrate that SOCE has essential and highly conserved roles in supporting normal heart physiology.

RESULTS

Heart specific suppression of *Stim* and *Orai* results in dilated cardiomyopathy

Drosophila Stim and *Orai* loss-of-function mutants fail to grow properly and die as second or third instar larvae, limiting their use in analysis of heart function. We therefore used inducible RNAi to suppress *Stim* and *Orai* expression specifically in the heart for many of our experiments. With this technique, RNAi transgenes under control of the inducible *UAS* promoter are activated by co-expression of a tissue specific *GAL4* driver. Importantly, RNAi was efficient and specific, since *Stim* and *Orai* RNAi driven by the ubiquitous *act-GAL4* driver suppressed *Stim* and *Orai* mRNA expression in first instar larvae by 72.67 ± 3.18% and 80 ± 2.65% (mean ± SEM), respectively, compared to non-targeting RNAi controls (Figure S1A). In addition, ubiquitous expression of *Stim* and *Orai* RNAi resulted in reduced growth and larval lethality (Figure S1B-F) similar to loss-of-function mutants, suggesting specific knockdown of the targeted gene products with little to no off-target effects.

To determine whether SOCE suppression is detrimental to cardiac function, we first evaluated the requirement for *Stim* and *Orai* in adult heart contractility using optical coherence tomography (OCT). Heart specific suppression of *Stim* and *Orai* using the heart-specific *tinC-GAL4* significantly increased the end-diastolic dimension (EDD) and end-systolic dimension (ESD) as compared with non-targeting RNAi controls (Figure 1A-H). Importantly, this resulted in significantly reduced fractional shortening (FS), a direct measure of the contractile strength of the heart, in *Stim* and *Orai* RNAi animals compared to controls (*Stim*, 42.28 ± 1.4%; *Orai*, 49.21 ± 3.11%; control, 88.73 ± 2.04%; Figure 1I, $p < 0.001$). These results demonstrating enlarged systolic and diastolic chamber dimensions and reduced fractional shortening are consistent with dilated cardiomyopathy in *Stim* and *Orai* RNAi animals. Similar results were also observed with *Stim* and *Orai* RNAi driven by a second heart specific driver, *4xhand-GAL4* (Figure 1J-R). Animals with *4xhand-GAL4* driven *Stim* and *Orai* RNAi again exhibited significantly larger EDD and ESD compared to nontargeting RNAi controls (Figure 1P,Q), and this resulted in

significantly reduced FS in *Orai* RNAi animals (Figure 1R). The decrease in FS was not significantly different in animals with *4xhand-GAL4* driven *Stim* RNAi; however, this may have resulted from only two out of eleven measurements that were similar to control. Neither *tinC-GAL4* nor *4xhand-GAL4* driven *Stim* and *Orai* RNAi significantly altered heart rates compared to controls (Figure S2A and B), nor were there any notable arrhythmias. Overall, heart specific suppression of *Stim* and *Orai* driven by two independent heart specific drivers resulted in dilated cardiomyopathy, demonstrating an essential function for both *Stim* and *Orai* in adult *Drosophila* cardiac function.

Heart specific *Stim* and *Orai* suppression delays development and causes early adult lethality

We next determined whether the contractility defects in *Stim* and *Orai* suppressed hearts negatively impact animal health and viability. In support of this, heart specific suppression of *Stim* and *Orai* driven with *tinC-GAL4* delayed larval development (Figure 2A and B), as significantly fewer *Stim* and *Orai* RNAi animals pupated on day five post-embryogenesis compared to controls (*Stim* RNAi, 8.667 ± 0.67%; *Orai* RNAi 6.67 ± 1.33%; non-targeting RNAi, 50.67 ± 6.67%, mean ± SEM; $p < 0.01$). This delay continued through to eclosion, when adult animals emerge from their pupal cases, again with only 12.33 ± 1.20% of *Stim* RNAi and 13 ± 2.08% of *Orai* RNAi animals' eclosing on day 9 as compared to 42.33 ± 6.49% of controls (Figure 2C and D). Trending delays were also noted with *4xhand-GAL4* driven *Stim* and *Orai* RNAi, though the effects were not statistically significant compared to controls (Figure 2E-H). The stronger effects with *tinC-GAL4* compared to *4xhand-GAL4* may be due to stronger activation of the *tin* promoter from embryogenesis through larval stages, whereas the *hand* promoter is more strongly engaged at later larval stages (Zhu et al., 2017). These delays in pupation and elcosion with heart-specific *Stim* and *Orai* RNAi suggest that SOCE function is required in the heart to support proper animal growth and development.

We next determined whether heart specific *Stim* and *Orai* suppression affects longevity by analyzing adult lifespan. In support of this, males with *tinC-GAL4* driven *Orai* RNAi died significantly earlier than nontargeting RNAi controls (Figure 3A and B), and the median lifespan of *tinC-GAL4* driven *Orai* RNAi animals was 39 ± 3.28 days compared to 52.5 ± 2.78 days nontargeting RNAi controls. Premature lethality of *tinC-GAL4* driven *Stim* animals did not reach statistical significance, possibly due to lower expression of *Stim* RNAi. Similar, though more profound, effects on adult lifespan were observed with *4xhand-GAL4* driven *Stim* and *Orai* RNAi (Figure 3C and D). The male median lifespan was 11 ± 1.73 and 13 ± 2.65 days for *4xhand-GAL4* driven *Stim* and *Orai* RNAi, respectively, compared to 43.64 ± 3.38 days for controls. Notably, effects on adult animal survival were significantly greater for *4xhand-GAL4* driven RNAi compared to *tinC-GAL4*, despite the greater effects on contractility seen with *tinC-GAL4*. This suggested that *4xhand-GAL4* driven RNAi may have had effects independent of heart function. In support of this, many of the *4xhand-GAL4* driven *Stim* and *Orai* RNAi animals had blistered or darkened and frayed wings, in some cases at the time of eclosion (Figure 3E). This likely reflects *4xhand-GAL4* driven RNAi expression in wing hearts (Togel et al., 2013; Togel et al., 2008), and further suggests a requirement for SOCE in muscle of cardiac origin. The blistered wing phenotype was not investigated further, but we did consider the possibility that wing damage may have contributed to the early lethality of the *4xhand-GAL4* driven RNAi animals by causing them to easily become stuck in the food or on the vial walls. To test this and more clearly determine whether lethality is attributable to dysfunction of the primary heart, we repeated adult survival experiments with *4xhand-GAL4* driven RNAi animals whose wings were removed at the time of eclosion. As shown in Figure 3F and G, wingless *Stim* and *Orai* RNAi animals indeed survived longer than those with wings, though these animals still died significantly earlier than corresponding wingless controls. Further, the survival of wingless *4xhand-GAL4* animals more closely resembled that of *tinC-GAL4* animals, suggesting

consistent early lethality due to abnormal heart function. Collectively, these results suggest that SOCE suppression pathologically impairs *Drosophila* cardiac function.

Heart specific Stim and Orai suppression causes abnormal larval and adult heart morphology

We next determined whether *Stim* and *Orai* suppression alters heart morphology and contractile myofibril organization in both larvae and adults. As shown in Figure 4A and B, third instar larval hearts from *tinC-GAL4* driven control RNAi animals exhibited evenly spaced myofibrils that uniformly wrapped circularly around the heart tube as revealed by actin staining. In contrast, myofibrils in *tinC-GAL4* driven *Stim* and *Orai* RNAi hearts were more widely spaced and less uniformly organized (indicated by arrows Figures 4C and D), suggesting SOCE suppression results in changes to heart structure. We also observed significant disruption of myofibril organization in adult hearts with *Stim* and *Orai* RNAi driven with *4xhand-GAL4,* as myofibrils in adult *4xhand-GAL4* driven *Stim* and *Orai* hearts were unevenly spaced and exhibited a higher incidence of longitudinal as opposed to circular orientation (indicated by arrows in Figure 4E-H). Disorganization and disruption of myofibril structure in larval and adult hearts resulting from SOCE suppression may arise due to defects heart contractility or development.

DISCUSSION

The functional importance of SOCE in cardiomyocytes remains unclear. Our results demonstrate essential roles for the SOCE pathway components Stim and Orai in normal *Drosophila* cardiac physiology, with pathway suppression resulting in pathologically dilated cardiomyopathy. Heart specific suppression of *Stim* or *Orai* in adult hearts resulted in increased end-diastolic and end-systolic dimensions with decreased fractional shortening, consistent with dilated cardiomyopathy, using two independent heart specific drivers. Importantly, previous studies in other animal models including mouse and zebrafish also demonstrated that knockdown or knockout of STIM1 or Orai1 results in dilated cardiomyopathy, suggesting highly conserved functions for SOCE in cardiomyocyte physiology (Collins et al., 2014; Horton et al., 2014; Parks et al., 2016; Volkers et al., 2012). The essential functions of SOCE in cardiomyocytes remain unclear but may involve roles for Stim and Orai in physiological cardiomyocyte growth, maintenance of sarcomere integrity, and support of SR and mitochondrial homeostasis (Collins et al., 2014; Voelkers et al., 2010; Volkers et al., 2012). Our results with *Drosophila* establish a new model for delineation of these roles, one in which combinatorial genetics and *in vivo* physiological analyses can be employed to directly test mechanistic functions.

A key advantage of *Drosophila* compared to other models is their simplified genetics. Most relevant to the functional analyses of SOCE, *Drosophila* only express single *Stim* and *Orai* orthologs, eliminating possible compensation by other isoforms such as STIM2 or Orai2 and Orai3 seen in vertebrate knockdown or knockout experiments. Additionally, in vertebrates STIM1 has been shown to interact with canonical transient receptor potential channels (TrpC) (Eder, 2017) and L-type voltage gated channels (Park et al., 2010; Wang et al., 2010), further complicating analyses of SOCE functions. However, the *Drosophila* TrpC orthologs, *Trp* and *Trpl*, are only expressed in cells of the phototransduction system and are therefore unlikely to contribute to SOCE functions in the heart (Hardie and Minke, 1992; Niemeyer et al., 1996). It

remains possible that *Drosophila* STIM may functionally interact with L-type voltage gated channels, and this possibility should be evaluated further. It is important to note that in our experiments, *Stim* and *Orai* RNAi both resulted in similar cardiac phenotypes, strongly suggesting that Orai-independent functions of Stim, or vice versa, are not significant factors.

Heart-specific suppression of *Stim* and *Orai* was detrimental to overall animal health, as it resulted in delayed development and early adult lethality. The developmental delay caused by *tinC-GAL4* driven RNAi may reflect defects in early cardiac development. Alternatively, compromised contractility in larvae may reduce circulation of essential metabolites or signaling factors such as the hormone ecdysone that induces larval molts and pupation. Interestingly, *tinC-GAL4* driven RNAi resulted in only modest reduction of adult lifespan, possibly reflecting the expression pattern of the *tin* promoter, which is highly expressed in the *Drosophila* heart during embryogenesis but drops significantly towards the end of embryogenesis with low expression levels in larval and adult stages (Jin et al., 2013). In support of this, *Stim* and *Orai* RNAi driven with *4xhand-GAL4*, which is expressed at lower levels starting at the end of embryogenesis but increases throughout the larval and adult stages, did not result in developmental delays but did cause significantly premature adult lethality. In addition, animals with *4xhand-GAL4* driven *Stim* and *Orai* RNAi exhibited blistered and severely damaged wings. Similar phenotypes have previously been attributed to defective function of wing hearts, which are secondary contractile organs that originate from pericardial cells and are located at the base of each wing. The main function of the wing hearts is to ensure proper hemolymph supply and circulation to the wings, in particular following eclosion when the wings are unfurled by a sudden influx of hemolymph propelled by these muscles (Togel et al., 2013; Togel et al., 2008). Importantly, wing hearts express *4xhand-GAL4* but not *tinC-GAL4* (Togel et al., 2013), likely explaining the presence of defective wings in animals with *Stim* and *Orai* driven by *4xhand-GAL4* but not *tinC-GAL4*. Additional differences in the tissue specificity of the *tinC-GAL4* versus *4xhand-GAL4* drivers, such as *4xhand-GAL4* expression in pericardial cells and lymph glands

(Han et al., 2006), may also contribute to the more severe effects on adult longevity seen with *4xhand-GAL4*.

Heart specific suppression of *Stim* and *Orai* also resulted in disrupted and disorganized myofibril structure in both larvae and adults. Larvae with *tinC-GAL4* driven *Stim* and *Orai* RNAi exhibited loosely packed myofibrils, and adults with *4xhand-GAL4* driven RNAi had significant myofibril disruption and disorganization compared to controls. These defects in cardiomyocyte structure are consistent with previous findings and may reflect SOCE functions in heart contractility, SR and mitochondrial homeostasis, or regulation of gene expression. For example, cardiac-restricted STIM1 knockout in mice resulted in SR dilation, induction of ER stress, and increased mitochondrial fission, suggesting that loss of SOCE may result in a stress response that alters cellular organization and suppresses cardiomyocyte contractility (Collins et al., 2014). In addition, Volkers et al found that loss of Orai1 in zebrafish hearts resulted in myofibril disaggregation and instability, most likely resulting from stretched or absent Z-disc structures (Volkers et al., 2012). Overall, the presence of disorganized myofibrils in conjunction with decreased contractile strength in *Stim* and *Orai* suppressed hearts suggests that loss of SOCE may disrupt myofibril growth and/or the ability to adapt to increasing demands.

Collectively, our results demonstrate an essential role for SOCE in normal cardiac physiology, and present how powerful genetic tools and *in vivo* analyses in *Drosophila* will allow us to define the mechanistic basis for this requirement. Further understanding of the molecular mechanisms underlying Ca^{2+} signaling dynamics in the heart will be essential to our understanding of cardiac pathophysiology and may lay the groundwork for development of novel therapeutic prevention and treatment options against cardiac disease.

MATERIALS AND METHODS

Fly Stocks

The following *Drosophila* stocks were obtained from the Bloomington *Drosophila* Stock Center: mCherry RNAi (35785; non-targeting control), GAL4 RNAi (35783; non-targeting control RNAi), *Stim* RNAi (27263), *Orai* RNAi (53333), and *act-GAL4* (3954). *tinC-GAL4* was obtained from Dr. Manfred Frausch (Friedrich Alexander University), and *4xhand-GAL4* was from Dr. Zhe Han (George Washington University School of Medicine). Flies were maintained on standard cornmeal agar food, and all crosses were carried out at 25ºC.

Adult Survival

Virgin female *tinC-GAL4* or *4xhand-GAL4* flies were crossed with male RNAi animals, and progeny were raised to adulthood at 25ºC to eclosion. On the day of eclosion, adult progeny were collected and separated based on sex into vials containing up to ten flies per vial, with a total of 20-30 flies per group. Flies were maintained at 25ºC throughout the course of the experiments. Every three days, the vials were checked for dead animals and surviving flies were transferred into new vials with fresh food. For wingless experiments, wings were removed immediately following eclosion on the day of adult collection.

Developmental Timing

Approximately 30-40 virgin female *tinC-GAL4* or *4xhand-GAL4* animals were mated with RNAi males for three days, at which time mated females were transferred into egg laying chambers that consisted of a 100ml plastic beaker with holes for air exchange affixed over a petri dish containing grape juice agar (Genesee Scientific). A dollop of yeast paste (active dry yeast mixed with water) was placed in the center of each grape juice agar plate to provide food. Animals were acclimated in the chambers for 24 hours, and then transferred to new plates for 4 hours at 25ºC for timed egg laying. After removing the females, plates with eggs were incubated

at 25ºC for an additional 24 hours. Hatched larvae were then transferred to vials with standard fly food, with up to 30 larvae per vial, and maintained at 25ºC through the course of the experiment. Vials were checked each day, and the numbers of newly formed pupae and eclosed adults were recorded.

RNA Isolation and RT-qPCR

Twenty to 30 first instar larvae were collected in 20µl cold Trizol and manually crushed with a pestle. Additional Trizol was then added to a total volume of 500µl, 100µl chloroform was added, and the aqueous layer containing extracted RNA was isolated. Extracted RNA was further purified with the RNeasy kit (Qiagen) and converted to cDNA using an S1000 Thermo Cycler (BioRad) with high capacity cDNA Reverse Transcription kit (ThermoFisher). Real-time quantitative polymerase chain reaction (RT-qPCR) was performed on a StepOnePlus RT-qPCR machine (Applied Biosystems) with each reaction consisting of triplicate samples containing iTaq Universal Probes Supermix (BioRad), pre-validated 6-carboxyfluorescein (FAM)-labeled Taqman probes (Applied Biosystems) against *Stim*, *Orai*, and *RPL32* (housekeeping gene), and template cDNA diluted per manufacturer's instructions. For quantification, triplicate cycle threshold (Ct) values were averaged and normalized to the *RPL32* Ct value to calculate ΔCt. The $\Delta(\Delta Ct)$ was determined by subtracting the control RNAi ΔCt value from the experimental ΔCt value, and fold changes expressed as $2^{-\Delta(\Delta Ct)}$. Fold changes are expressed as a percentage of expression compared to non-targeting RNAi control.

Heart Dissection, Staining, and Confocal Imaging

Hearts from third instar larvae of five-day old adults were dissected and fixed as previously described (Alayari et al., 2009). In brief, for adults the ventral abdomens and underlying tissues were removed to expose the contracting heart while bathed in oxygenated artificial *Drorophila* hemolymph (ADH; 108 mM NaCl, 5 mM KCl, 2 mM $CaCl_2$, 8 mM $MgCl_2$, 1

mM NaH_2PO_4, 4 mM $NaHCO_3$, 10 mM sucrose, 5 mM trehalose, and 5 mM HEPES (pH 7.1). Hearts were then fully relaxed by exchange with fresh ADH containing 10 mM EGTA. Larvae were pinned to Sylgard coated dishes at their anterior and posterior, and a slit was cut along the ventral midline in the presence of oxygenated ADH. Lateral cuts were then made along the sides of the animals, and the resulting cuticle flaps were pinned to expose the internal organs. The gut was removed to expose the beating hearts, which was then relaxed with ADH containing 10 mM EGTA. Dissected adults and larvae were both fixed for 20 min at room temperature in PBS containing 4% paraformaldehyde. Following three 10 min washes in PBS containing 0.1% Triton X-100 (PBSTx) with gentle rotation, the samples were incubated in PBSTx containing 1.0 µM Alexa Fluor 488 Phalloidin (ThermoFisher) for one hour at room temperature with gentle shaking. Samples were again washed three times in PBSTx at room temperature, and mounted on glass slides and coverslips with Vectashield (Vectashield Laboratories) as described (Alayari et al., 2009). Samples were imaged with a Nikon A1R confocal microscope using 10X, 0.45 N.A. and 40X, 1.3 NA objectives. Phalloidin was excited with a 488 nm laser. Z-stacks at 1 µm intervals were collected and images are presented as maximum intensity projections encompassing the whole heart for larvae or the dorsal half of the heart for adults to avoid the ventral layer of skeletal muscle.

Optical Coherence Tomography (OCT)

Adult heart contractility was analyzed using a custom-built OCT apparatus as previously described (Wolf et al., 2006). In brief, five-day old males were briefly anesthetized with CO_2, embedded in a soft gel support, and allowed to fully awaken based on body movement. Animals were first imaged in B-mode in the longitudinal orientation to identify the A1 segment of the heart chamber. They were then imaged transversely in M-mode for 3 sec, and multiple M-modes were recorded for each fly. Animals were then re-imaged in B-mode to endure proper orientation of the heart chamber. M-modes were processed in ImageJ by referencing to a 150

μm standard. End-diastolic dimension (EDD), end-systolic dimensions (ESD), and heart rate were calculated directly from the processed M-mode traces. Percent fractional shortening (FS) was calculated as (EDD-ESD) / EDD x 100.

REFERENCES

Abraham, D.M., and Wolf, M.J. (2013). Disruption of sarcoendoplasmic reticulum calcium ATPase function in Drosophila leads to cardiac dysfunction. PLoS One *8*, e77785.

Alayari, N.N., Vogler, G., Taghli-Lamallem, O., Ocorr, K., Bodmer, R., and Cammarato, A. (2009). Fluorescent labeling of Drosophila heart structures. Journal of visualized experiments : JoVE.

Benard, L., Oh, J.G., Cacheux, M., Lee, A., Nonnenmacher, M., Matasic, D.S., Kohlbrenner, E., Kho, C., Pavoine, C., Hajjar, R.J*., et al.* (2016). Cardiac Stim1 Silencing Impairs Adaptive Hypertrophy and Promotes Heart Failure Through Inactivation of mTORC2/Akt Signaling. Circulation *133*, 1458-1471; discussion 1471.

Bers, D.M. (2002). Cardiac excitation-contraction coupling. Nature *415*, 198-205.

Collins, H.E., He, L., Zou, L., Qu, J., Zhou, L., Litovsky, S.H., Yang, Q., Young, M.E., Marchase, R.B., and Chatham, J.C. (2014). Stromal interaction molecule 1 is essential for normal cardiac homeostasis through modulation of ER and mitochondrial function. Am J Physiol Heart Circ Physiol *306*, H1231-1239.

Eder, P. (2017). Cardiac Remodeling and Disease: SOCE and TRPC Signaling in Cardiac Pathology. Advances in experimental medicine and biology *993*, 505-521.

Han, Z., Yi, P., Li, X., and Olson, E.N. (2006). Hand, an evolutionarily conserved bHLH transcription factor required for Drosophila cardiogenesis and hematopoiesis. Development (Cambridge, England) *133*, 1175-1182.

Hardie, R.C., and Minke, B. (1992). The trp gene is essential for a light-activated Ca2+ channel in Drosophila photoreceptors. Neuron *8*, 643-651.

Horton, J.S., Buckley, C.L., Alvarez, E.M., Schorlemmer, A., and Stokes, A.J. (2014). The calcium release-activated calcium channel Orai1 represents a crucial component in hypertrophic compensation and the development of dilated cardiomyopathy. Channels (Austin, Tex) *8*, 35-48.

Hulot, J.S., Fauconnier, J., Ramanujam, D., Chaanine, A., Aubart, F., Sassi, Y., Merkle, S., Cazorla, O., Ouille, A., Dupuis, M*., et al.* (2011). Critical role for stromal interaction molecule 1 in cardiac hypertrophy. Circulation *124*, 796-805.

Jin, H., Stojnic, R., Adryan, B., Ozdemir, A., Stathopoulos, A., and Frasch, M. (2013). Genome-wide screens for in vivo Tinman binding sites identify cardiac enhancers with diverse functional architectures. PLoS genetics *9*, e1003195.

Kranias, E., and Bers, D. (2007). Calcium and Cardiomyopathies, Vol 45.
Lacruz, R.S., and Feske, S. (2015). Diseases caused by mutations in ORAI1 and STIM1. Ann N Y Acad Sci *1356*, 45-79.

Limas, C.J., Olivari, M.T., Goldenberg, I.F., Levine, T.B., Benditt, D.G., and Simon, A. (1987). Calcium uptake by cardiac sarcoplasmic reticulum in human dilated cardiomyopathy. Cardiovascular research *21*, 601-605.

Luo, X., Hojayev, B., Jiang, N., Wang, Z.V., Tandan, S., Rakalin, A., Rothermel, B.A., Gillette, T.G., and Hill, J.A. (2012). STIM1-dependent store-operated Ca(2)(+) entry is required for pathological cardiac hypertrophy. Journal of molecular and cellular cardiology *52*, 136-147.

MacLeod, K.T. (2016). Recent advances in understanding cardiac contractility in health and disease. F1000Research *5*.

McKenna, W.J., Maron, B.J., and Thiene, G. (2017). Classification, Epidemiology, and Global Burden of Cardiomyopathies. Circulation research *121*, 722-730.

Niemeyer, B.A., Suzuki, E., Scott, K., Jalink, K., and Zuker, C.S. (1996). The Drosophila light-activated conductance is composed of the two channels TRP and TRPL. Cell *85*, 651-659.

Park, C.Y., Shcheglovitov, A., and Dolmetsch, R. (2010). The CRAC channel activator STIM1 binds and inhibits L-type voltage-gated calcium channels. Science (New York, NY) *330*, 101-105.

Parks, C., Alam, M.A., Sullivan, R., and Mancarella, S. (2016). STIM1-dependent Ca(2+) microdomains are required for myofilament remodeling and signaling in the heart. Sci Rep *6*, 25372.

Piazza, N., and Wessells, R.J. (2011). Drosophila models of cardiac disease. Prog Mol Biol Transl Sci *100*, 155-210.

Putney, J.W. (2011). The physiological function of store-operated calcium entry. Neurochem Res *36*, 1157-1165.

Putney, J.W. (2018). Forms and functions of store-operated calcium entry mediators, STIM and Orai. Adv Biol Regul *68*, 88-96.

Rotstein, B., and Paululat, A. (2016). On the Morphology of the Drosophila Heart. Journal of Cardiovascular Development and Disease *3*, 15.

Smyth, J.T., Hwang, S.Y., Tomita, T., DeHaven, W.I., Mercer, J.C., and Putney, J.W. (2010). Activation and regulation of store-operated calcium entry. J Cell Mol Med *14*, 2337-2349.

Togel, M., Meyer, H., Lehmacher, C., Heinisch, J.J., Pass, G., and Paululat, A. (2013). The bHLH transcription factor hand is required for proper wing heart formation in Drosophila. Developmental biology *381*, 446-459.

Togel, M., Pass, G., and Paululat, A. (2008). The Drosophila wing hearts originate from pericardial cells and are essential for wing maturation. Developmental biology *318*, 29-37.

Voelkers, M., Salz, M., Herzog, N., Frank, D., Dolatabadi, N., Frey, N., Gude, N., Friedrich, O., Koch, W.J., Katus, H.A.*, et al.* (2010). Orai1 and Stim1 regulate normal and hypertrophic growth in cardiomyocytes. Journal of molecular and cellular cardiology *48*, 1329-1334.

Volkers, M., Dolatabadi, N., Gude, N., Most, P., Sussman, M.A., and Hassel, D. (2012). Orai1 deficiency leads to heart failure and skeletal myopathy in zebrafish. J Cell Sci *125*, 287-294.

Wang, Y., Deng, X., Mancarella, S., Hendron, E., Eguchi, S., Soboloff, J., Tang, X.D., and Gill, D.L. (2010). The calcium store sensor, STIM1, reciprocally controls Orai and CaV1.2 channels. Science (New York, NY) *330*, 105-109.

Wolf, M.J., Amrein, H., Izatt, J.A., Choma, M.A., Reedy, M.C., and Rockman, H.A. (2006). Drosophila as a model for the identification of genes causing adult human heart disease. Proceedings of the National Academy of Sciences of the United States of America *103*, 1394-1399.

Zhu, J.Y., Fu, Y., Nettleton, M., Richman, A., and Han, Z. (2017). High throughput in vivo functional validation of candidate congenital heart disease genes in Drosophila. eLife *6*.

ACKNOWLEDGEMENTS

This work was supported by funding from the Collaborative Health Initiative Research Program to C.E.P. and J.T.S. and from the National Institutes of Health to M.J.W.

FIGURE LEGENDS

Figure 1. Heart specific suppression of *Stim* and *Orai* results in dilated cardiomyopathy.

A-C. Representative OCT longitudinal B-mode images of five day old adult male flies with *tinC-GAL4* driven nontargeting control, *Stim*, and *Orai* RNAi during systole (upper panels) and diastole (lower panels). Arrowheads indicate the heart in systole images**.** Scalebar, 244 µm. **D-F** Representative m-mode images from *tinC-GAL4* driven nontargeting control, *Stim*, and *Orai* RNAi with yellow lines depicting systole and red lines diastole. EDD (**G**), ESD (**H**), and FS (**I**) were calculated from M-mode recordings of five day old animals, and each symbol represents a measurement from a single animal (****, $p < 0.0001$, One-way ANOVA with Tukey's Multiple Comparison). **J-L.** Representative OCT longitudinal B-mode images of five day old adult male flies with *4xhand-GAL4* driven nontargeting control, *Stim*, and *Orai* RNAi during systole (upper panels) and diastole (lower panels). Arrowheads indicate the heart in systole images**. M-O** Representative m-mode images from *hand-GAL4* driven nontargeting control, *Stim*, and *Orai* RNAi with yellow lines depicting systole and red lines diastole. EDD (**P**), ESD (**Q**), and FS (**R**) were calculated from M-mode recordings of five day old animals, and each symbol represents a measurement from a single animal (****, $p < 0.0001$; ***, $p < 0.005$; **, $p < 0.05$; One-way ANOVA with Tukey's Multiple Comparison.

Figure 2. Heart specific suppression of *Stim* and *Orai* delays animal development.

A. Plot of the total number of pupae formed, expressed as a percent of the total number of larvae analyzed (25-50 per group), on each of the indicated days post-embryo hatching for *tinC-GAL4* driven *Stim*, *Orai*, and nontargeting control RNAi. Data are mean ± SEM from three independent experiments. **B.** Comparison of percent pupated on day 5 post-hatching for *tinC-GAL4* driven *Stim*, *Orai,* and non-targeting control RNAi from three independent replicates (*, $p = 0.0007$, **, $p = 0.0005$; One-way ANOVA with Tukey's Multiple Comparisons Test). **C.** Plot of the total *tinC-GAL4* driven *Stim*, *Orai*, and nontargeting control RNAi animals that eclosed on

each of the indicated days post-embryo hatching, as a percent of the total pupated animals. Data are mean ± SEM from three independent experiments. **D.** Comparison of percent eclosed on day 9 post-hatching for *tinC-GAL4* driven *Stim*, *Orai* and non-targeting control RNAi (*, p = 0.0049, **, p = 0.0044; One-way ANOVA with Tukey's Multiple Comparisons Test). **E.** Plot of the total number of pupae formed, expressed as a percent of the total number of larvae analyzed (25-50 per group), on each of the indicated days post-embryo hatching for *4xhand-GAL4* driven *Stim*, *Orai*, and nontargeting control RNAi. Data are mean ± SEM from three independent experiments. **F.** Comparison of percent pupated on day 5 post-hatching for *4xhand-GAL4* driven *Stim*, *Orai,* and non-targeting control RNAi. **G.** Plot of the total *4xhand-GAL4* driven *Stim*, *Orai*, and nontargeting control RNAi animals that eclosed on each of the indicated days post-embryo hatching, as a percent of the total pupated animals. Data are mean ± SEM from three independent experiments. **H.** Comparison of percent eclosed on day 9 for *4xhand-GAL4* driven *Stim*, *Orai* and non-targeting control RNAi.

Figure 3: Heart specific suppression of *Stim* and *Orai* results in early adult lethality

A. Representative survival curves in days post-embryogenesis of adult males with *tinC-GAL4* driven *Stim* RNAi (blue triangles), *Orai* RNAi (red squares), and nontargeting control RNAi (black line). **B.** Adult male median lifespan (MLS) for *tinC-GAL4* driven *Stim*, and *Orai*, and nontargeting control RNAi from three independent survival experiments. MLS was significantly decreased for *Orai* ($p < 0.05$; One-way ANOVA with Tukey's Multiple Comparisons Test) but not *Stim* compared to control **C.** Representative survival curves in days post-eclosion of adult males with *4xhand-GAL4* driven *Stim* RNAi (blue triangles), *Orai* RNAi (red squares), and nontargeting control RNAi (black line). **D.** Adult male median lifespan (MLS) for *4xhand-GAL4* driven *Stim*, *Orai*, and nontargeting control RNAi from three independent survival experiments. (**, p = 0.0002; *, p = 0.003; One-way ANOVA with Tukey's Multiple Comparisons Test. **E.** Representative images of blistered and damaged wings (indicated by arrows) of adult males on

day of eclosion for *4xhand-GAL4* driven *Stim*, *Orai*, and nontargeting RNAi control animals. **F.** Representative survival curves in days post-eclosion of adult males with *4xhand-GAL4* driven *Stim* RNAi (blue triangles), *Orai* RNAi (red squares), and nontargeting control RNAi (black line) with wings removed on the day of eclosion. **G.** Adult male median lifespan (MLS) for *4xhand-GAL4* driven *Stim*, *Orai*, and nontargeting control RNAi with wings removed on the day of eclosion from three independent experiments (*, $p = 0.0032$; **, $p = 0.0026$; One-way ANOVA with Tukey's Multiple Comparisons Test).

Figure 4: Heart specific suppression of *Stim* and *Orai* results in defects in larval and adult heart morphology

A. Representative image of a control third instar larval heart stained with Phallodin to visualize actin. The box denotes the region shown in the lower high resolution images. **B-D.** Representative high resolution images of the region around the second ostium from *tinC-GAL4* driven nontargeting control, *Stim*, and *Orai* RNAi hearts. Arrowheads point to ostia, and arrows point to disorganized myofibrils (n=4-7 hearts per group). **E.** Representative image of an adult male control heart stained with Phallodin to visualize actin. The box denotes the region shown in the lower high resolution images. **F-H.** Representative high resolution images of the region around the second ostium from *4xhand-GAL4* driven nontargeting control, *Stim*, and *Orai* RNAi hearts. Arrowheads point to ostia, and arrows point to disorganized myofibrils (n=7-10 hearts per group).

Figure 1

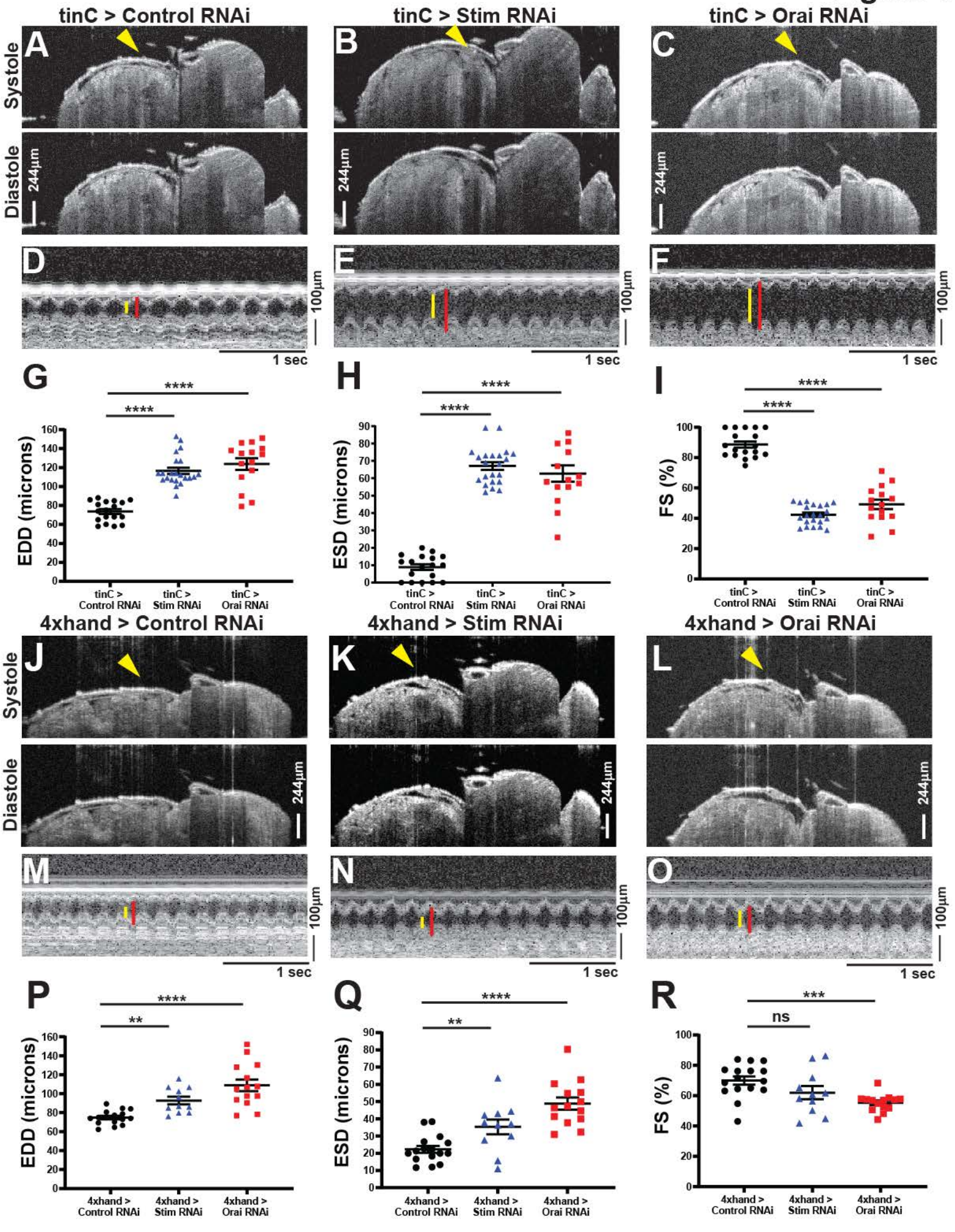

Figure 2

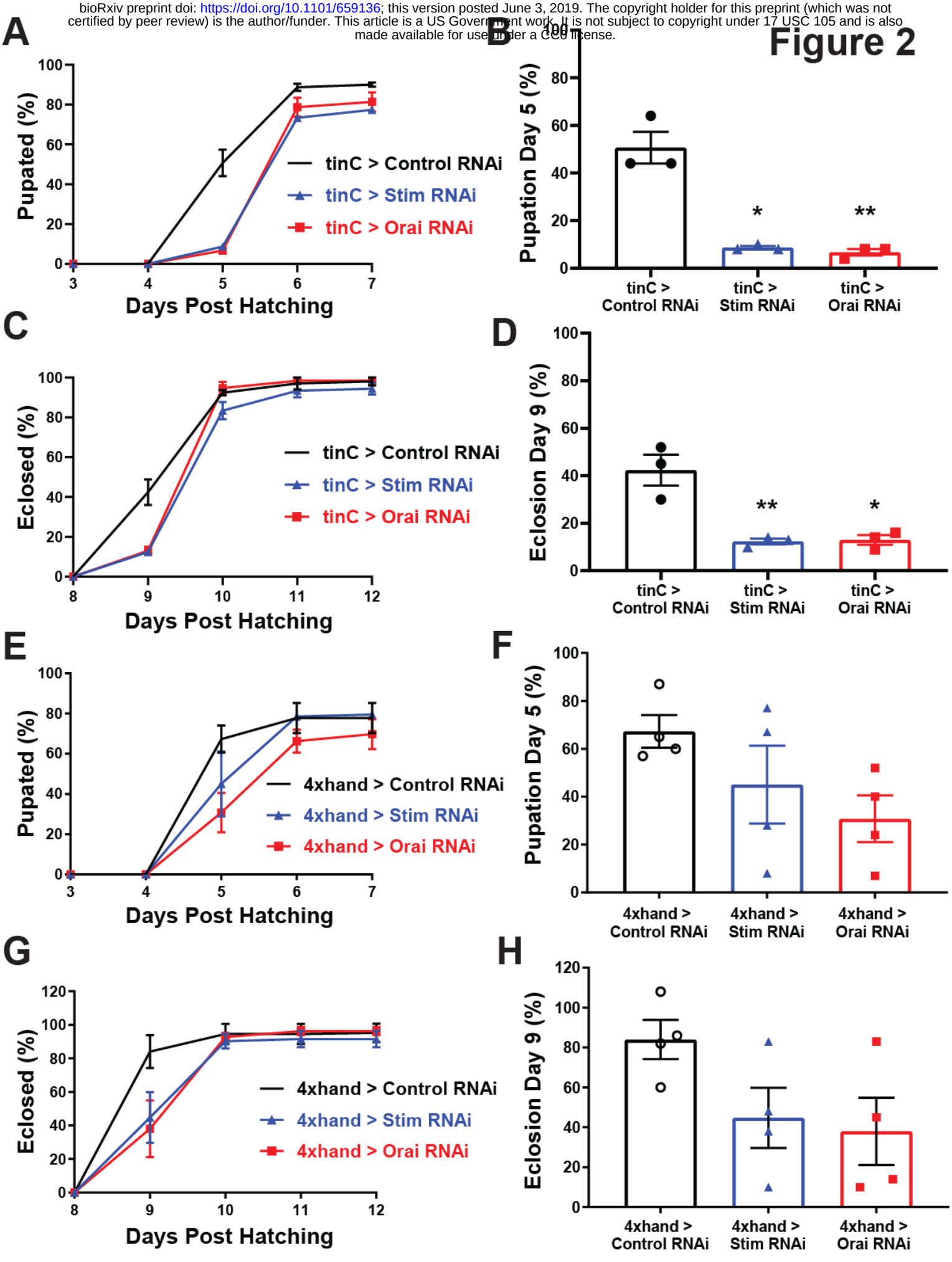

Figure 3

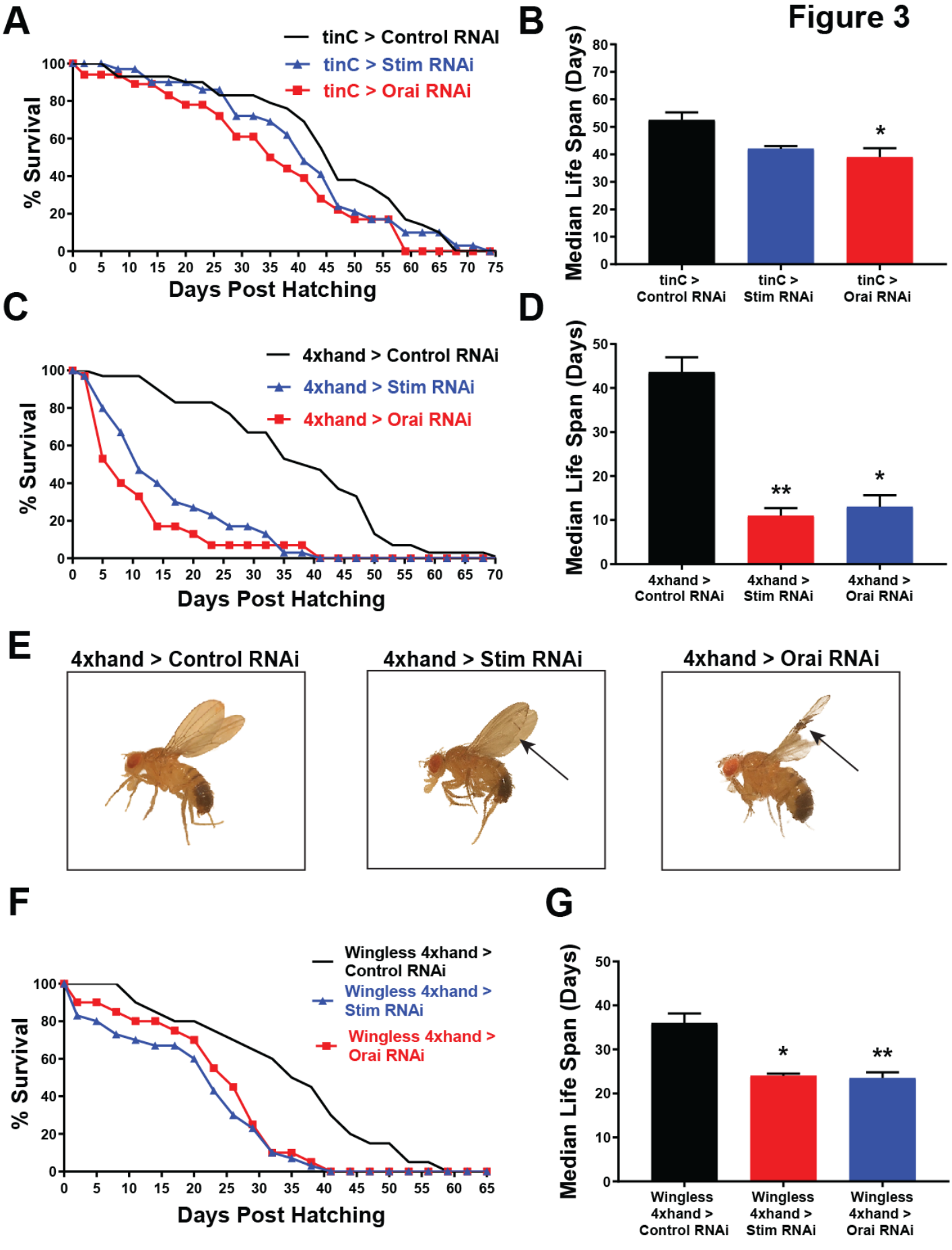

Figure 4